Analog spin simulators: How to keep the amplitude homogeneous

W. Verstraelen,[1,*] P. Deuar,[2] M. Matuszewski,[2] and T.C.H. Liew[1]

[1] *Division of Physics and Applied Physics, School of Physical and Mathematical Sciences, Nanyang Technological University, Singapore 637371, Singapore*

[2] *Institute of Physics, Polish Academy of Sciences, Al. Lotników 32/46, Warsaw PL-02-668, Poland*

(Received 8 June 2023; revised 7 December 2023; accepted 5 February 2024; published 29 February 2024)

A setup that simulates ground states of spin graphs would allow one to solve computationally hard optimization problems efficiently. Current optical setups to this goal have difficulties decoupling the amplitude and phase degrees of freedom of each effective spin, which risks that the resultant mapping will be invalid, a problem known as amplitude heterogeneity. Here, we propose a setup with coupled active optical cavity modes, where this problem is eliminated through their particular geometric arrangement. Acting as an effective Monte Carlo solver, the ground state can be found exactly. By tuning a parameter, the setup solves *XY* or Ising problems.

DOI: 10.1103/PhysRevApplied.21.024057

I. INTRODUCTION

A. Analog spin simulators

Over the course of a few decades, the rise and spread of digital computers has transformed society completely. These rely mainly on Turing machines on a von Neumann architecture, with continuous improvement until recently according to Moore's law. It has become clear however, that they are limited for certain tasks, leading to the conceptualization of alternative setups. These include gate-based quantum computing [1] and neural networks [2] as well as analog simulation (either classical or quantum [3]). Simulation refers to the ability of an accessible system to reproduce the physics of a less accessible one. While such a "less accessible system" may be studied for its own sake, it can also have applications. This is the case for simulating spin models on a graph. In fact, in the presence of frustration, these correspond to spin-glass systems [4] for which the determination of the ground state is an (NP- and QMA-) hard problem, needing a potentially exponential amount of time both in a classical or quantum setup [5]. That also implies that simulating these spin models and finding their ground state would allow one to solve all other problems in these classes (such as traveling salesman or knapsack problems) with only polynomial overhead [6]. It has in fact been shown that all quantum computing tasks can be recast efficiently in instances of this problem through so-called adiabatic quantum computing [7].

There has been much interest to simulating such spin graphs especially with optics, because of their ease of access and ability to operate away from equilibrium [8–11]. Despite alternatives [12–15], the by far most commonly proposed setup uses a mapping from optical phase to spin orientation. By default, phase in an oscillator has a freedom of 2π, mapping straightforwardly to the orientation of an *XY* spin [16–19]. Driving with degenerate parametric oscillators reduces the phase to only a few possible values (usually two), as in an Ising spin. These are the coherent Ising machines and similar setups [8,20–24] or Potts model solvers [25]; notably, some superconducting qubits are implemented similarly. Using time-multiplexing and electronic overheads, effective system sizes up to 10^4 have been achieved [26], while more recent schemes consider elimination of the electronics [21].

In this work, we will introduce an alternative flexible similator, depicted in Fig. 1, that overcomes a critical limitation of many such previous setups.

B. The problem: Amplitude heterogeneity

In the above systems, a linear—but often dissipative—direct coupling between the oscillators faithfully maps the spin model to the coupling between on-site phases.

However, the analog simulators typically have more degrees of freedom than the original spin model. To avoid affecting the dynamics, their value should remain fixed. In particular, for optical simulators, spin variables $s_i = e^{i\theta_i}$ are represented by a local order parameter $\psi_i = |\psi_i| e^{i\theta_i}$, and consequently the spin Hamiltonians

$$H_{\text{spin}} = -\,\text{Re}\sum_{\langle ij\rangle} \pm s_i^* s_j = -\sum_{\langle ij\rangle} \pm\cos\left(\theta_i - \theta_j\right) \qquad (1)$$

*wouter.verstraelen@ntu.edu.sg

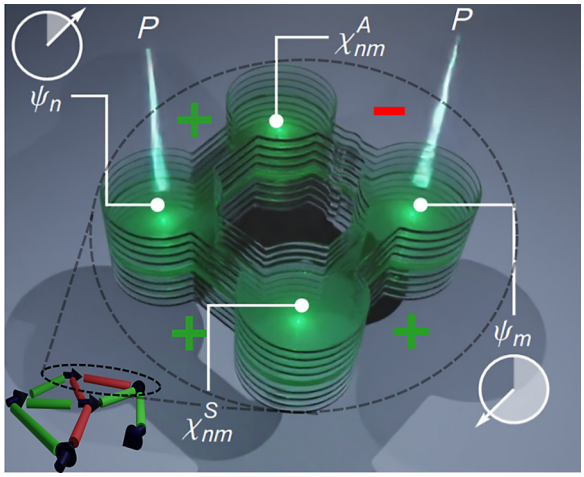

FIG. 1. Depiction of the proposed scheme with polariton micropillars acting as coupled cavities. Two "spin" sites ψ_n and ψ_m are coherently coupled through the undriven "connecting" χ^S_{nm} and χ^A_{nm}. The bump in the coupling between χ^A_{nm} and ψ_m indicates its different path length giving this coupling a strength $-J$, while the others are all $+J$. Inset: $\psi_{n,m}$ correspond to a generic pair of connected spins in the graph, with either ferromagnetic or antiferromagnetic coupling.

are mapped on

$$H_{\text{analog}} = -\,\text{Re}\sum_{\langle ij\rangle} \pm\psi_i^*\psi_j$$
$$= -\sum_{\langle ij\rangle} \pm|\psi_i||\psi_j|\cos(\theta_i-\theta_j), \qquad (2)$$

where $\langle nm\rangle$ are the edges of the graph and $\pm$ is positive (negative) for ferromagnetic (antiferromagnetic) couplings. Whereas in the XY case the phase differences can have arbitrary values, in the Ising case, we have $\cos(\theta_n-\theta_m)=\pm1$. See also the illustration in Fig. 2.

When the amplitudes $|\psi_i|$ are not kept fixed, it is easy to see that the spectra, and thus ground-state configurations between Eqs. (1) and (2) will generally not match. This critical problem, "broken mapping due to amplitude heterogeneity" [8,10] is known to ultimately invalidate the spin solution [27] and the simulation schemes.

It is unsurprising, in a sense, that the computationally complex spin-glass problem cannot be equivalent to the completely linear problem that arises when the spins are replaced by harmonic oscillators, such as noninteracting photons. Two mechanisms are known that can somewhat mitigate this problem. The first one is to include optical nonlinearities, such as in exciton polaritons [16], so that a steady state is found by the nonlinear dynamics well above threshold [27]. A clever choice of a sufficiently strong nonlinearity can be found, to have the strongest improvement, but it will generally be insufficient by itself to overcome heterogeneity [27,28]. The second mechanism is adapting

FIG. 2. Amplitude heterogeneity. Consider an Ising model with $H=-\sum_{ij}J_{ij}s_is_j$ on a triangular graph with two ferromagnetic ($J_{ij}=1$) and one antiferromagnetic ($J_{ij}=-1$) coupling, depicted in green (red), for variables $s=\pm1$. It is frustrated: no Ising configuration can satisfy all couplings simultaneously. One of the degenerate ground states is shown. However, the mapping from spins s_i to complex amplitudes ψ_i is not exact, since the absolute values $|\psi_i|$ are not normalized to unity. This leads to lower-energy solutions, which are unphysical in terms of the original Ising model. In this work, a scheme is introduced that avoids the occurrence of such amplitude heterogeneity.

the optical driving at every site continuously in a feedback loop to force a uniform intensity. This seems an intuitive fix, however, it is cumbersome on its own, as it introduces additional overhead, with potentially the need for an additional separation of timescales, and the necessity to estimate the threshold value [29,30]. Again, such a mechanism will give some moderate improvements in accuracy, but insufficient to overcome the bias from amplitude heterogeneity completely: even an exponentially slow operation will often fail to converge to the actual spin ground state [31].

One may thus wonder if this amplitude heterogeneity is a fundamental issue of any optical spin solver, or if a scheme can be devised to bypass it directly.

C. This work

Here, we will answer the latter question affirmatively and demonstrate the existence of such an analog simulation scheme without amplitude heterogeneity. We show explicitly how it can be implemented in a system of coupled optical cavities experiencing gain and saturable absorption, such as those realizable with exciton-polariton micropillars [32–34]. Such systems are already considered reasonable candidates for analog simulators given their fast operation time and accessibility [35,36] and are especially studied for XY spin models [25,29,37–39]. We consider a scheme where spin orientations are mapped to the phases of cavity fields. Its unique feature is that the coupling between the spin-mapping cavities happens through a pair of intermediate cavities with coherent Josephson coupling in such a way that the particle flow between effective spins is exactly canceled—as we will show—and thus amplitude heterogeneity is avoided. Depending on a parameter, XY or Ising graphs are simulated. Our scheme

works in a pulsed-operation mode [40,41], as an effective Monte Carlo solver across different spin solutions; with a feedback system that ensures that the spin ground-state solution survives. This paper is organised as follows: in Sec. II we introduce the scheme, and show how it can represent all spin configurations faithfully, i.e. with a homogeneous amplitude. In the next Sec. III, we then describe the approach to find the ground state of the spin model effectively. We conclude in Sec. IV.

II. A SCHEME THAT KEEPS THE AMPLITUDE HOMOGENEOUS

It has been known that nonlinear oscillators with direct coupling generally tend to synchronize according to various models [37,42,43]. However, it is believed that the resulting phase configuration matches a spin ground state only in the case of purely dissipative couplings [37], a correlated loss process on neighboring sites. It is clear that a lack of symmetry in such a setup generally affects the intensities inhomogeneously. Here, we explicitly look for an alternative setup, unaffected by these considerations.

Consider first two cavities with complex mean-field amplitudes, ψ_1 and ψ_2, which will represent the spins. Each cavity is coupled to two auxiliary "connecting" cavities with complex amplitudes, χ_{12}^S and χ_{12}^A, ("symmetric" and "antisymmetric" for the effective coupling they will later induce), with the connectivity illustrated in Fig. 1.

We exploit the possibility to control the sign of the Josephson coupling between modes [44], but only need real (Hermitian) values, typically dominant in physical realizations [45]. The evolution of the system is described by complex Ginzburg-Landau equations [46,47] in the tight-binding limit [45,48]

$$\begin{aligned} i\frac{\partial \psi_{1,2}}{\partial t} &= i\left(\frac{P-\gamma}{2} - \Gamma_{\rm NL}|\psi_{1,2}|^2\right)\psi_{1,2} - J\left(\chi_{12}^S \pm \chi_{12}^A\right), \\ i\frac{\partial \chi_{12}^{S,A}}{\partial t} &= i\left(\frac{-\gamma}{2} - \Gamma'_{\rm NL}|\chi_{12}^{S,A}|^2\right)\chi_{12}^{S,A} - J\left(\psi_1 \pm \psi_2\right), \end{aligned} \tag{3}$$

where the $\pm$ sign takes a $-$ value for the coupling between ψ_2 and χ_{12}^A only, and $+$ sign otherwise. Here we consider the case of a local gain P applied to the cavities $\psi_{1,2}$, a local decay γ (dissipation) on all cavities, and nonlinear losses (modeling gain saturation or saturable absorption into the system, and/or incoherent scattering and two-photon absorption out of the system). $\Gamma_{\rm NL}$ and $\Gamma'_{\rm NL}$ are applied to the two sets of modes, respectively. The choice of the coupling scheme (Fig. 1) ensures that, in the absence of the loss processes on the auxiliary modes, there is no effective coupling between the "spin" modes ψ_1 and ψ_2. This can be seen by considering (in the limit $\gamma = 0$, $\Gamma'_{\rm NL} = 0$):

$$i\left.\frac{\partial^2 \psi_{1,2}}{\partial t^2}\right|_{\rm coupling} = -J\left(\frac{\partial \chi_{12}^S}{\partial t} \pm \frac{\partial \chi_{12}^A}{\partial t}\right) = -2iJ^2\psi_{1,2}. \tag{4}$$

That is, ψ_1 and ψ_2 can evolve independently, allowing for solutions where $|\psi_1| \equiv |\psi_2|$. Intuitively, transport from ψ_1 to ψ_2 is suppressed by destructive interference of the χ_1 and χ_2 paths. This prevents the occurrence of amplitude heterogeneity, and hence of broken mapping. In the presence of $\gamma \neq 0$, one finds that the stationary solutions of the system also fix $|\psi_1|^2 = |\psi_2|^2$. Specifically,

$$\chi_{12}^{S,A} = \frac{2Ji}{\gamma}\left(\psi_1 \pm \psi_2\right), \tag{5}$$

$$I_0 := |\psi_1|^2 = |\psi_2|^2 = \frac{P-\gamma}{2\Gamma_{\rm NL}} - \frac{4J^2}{\gamma\Gamma_{\rm NL}}. \tag{6}$$

Note that the phases of $\psi_{1,2}$ can still be freely chosen.

A. *XY* graphs

We now consider a graph network. At its nodes, we consider "spin" sites ψ_n and the edges of the graph are implemented by the pair of "connecting" cavities $\chi_{nm}^{S/A}$ with the connectivity scheme from Fig. 1. For generality, we will consider arbitrarily connected graphs. In practice, by coupling neighboring cavities one may only be able to access planar graphs, however every other, potentially all-to-all connected graph can be mapped onto these [49,50]. In addition, it is in principle possible to couple spatially remote cavities via external optics [38] or a mask [18].

For a "spin" site ψ_m connected to $n_{\rm nb}^m$ neigboring spin sites, Eq. (6) generalizes to $I_0^{(m)} = (P_m - \gamma)/(2\Gamma_{\rm NL}) - 4n_{\rm nb}^m J^2/(\gamma\Gamma_{\rm NL})$. In general, this value would not be constant for homogenous $P_m = P$, as $n_{\rm nb}^m$ varies across main sites m in a generic graph. However, in order to avoid any bias, we require $I_0^{(m)} = I_0$. We can ensure this condition in different ways. The first approach comprises of extending the original spin graph with "extra" dangling (single neighbor) spins that do not affect the ground state in the subgraph corresponding to the original configuration; and implementing the scheme based on this extended graph.

Figure 3(a) shows a polar plot of the resulting state of a typical graph, obtained by solving numerically from an initial low-intensity random complex noise state and time evolving toward a stationary state. In this calculation the nonlinear loss on the "connecting" sites is set to zero ($\Gamma'_{\rm NL} = 0$). We find that the "main" sites (red) rapidly grow in intensity and equilibrate at the analytically expected value of I_0, while preserving their phase from the initial noise. The "extra" sites (green) show a similar behavior,

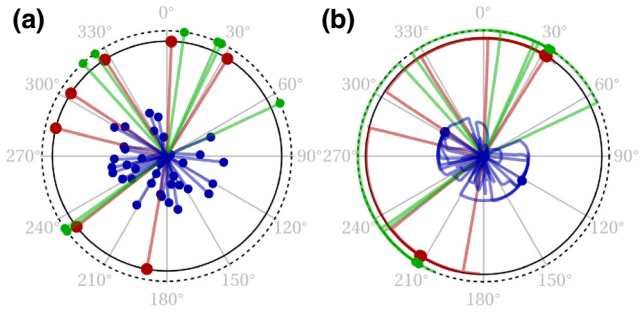

FIG. 3. Absolute amplitude (radial component) and phase (angles) for a random graph composed of seven "spin" sites (red), eight "extra" sites (green) that ensure the main sites have all the same number of neighbors (four for the considered example), and "connecting" sites (blue). Time evolution is shown with a linearly increasing opacity, up to a stationary state denoted by the spots. (a) *XY*-type behavior where the "spin" sites adopt arbitrary phases; (b) Ising-type behavior where the "spin" site phases become binary. The black circle corresponds to the analytically predicted magnitude $\sqrt{I_0}$. Parameters: $J/\Gamma_{\rm NL} = 0.5$; $P/\Gamma_{\rm NL}, = 12 + 2$; $\gamma/\Gamma_{\rm NL} = 4$; and $\Gamma'_{\rm NL}/\Gamma_{\rm NL} = 0$ in the *XY* case (a) or Ising case (b). The graph has a 50% connectivity, all antiferromagnetic to ensure frustration to make it nontrivial. Even though the "extra" sites are used, we have added contribution +2 to $P/\Gamma_{\rm NL}$ that compensates exactly for the losses $8n_{\rm NB}J^2/\gamma$ through the neighboring sites.

although they settle at slightly higher intensity as they have only one connected neighbor each. The "connecting" sites (blue) settle with a variety of different amplitudes and phases. The "spin" sites correspond effectively to a valid configuration of the corresponding *XY* graph, since they each have $\mathcal{U}(1)$ freedom in the phases, while their intensities are the same. Similar behavior to Fig. 3(a) was observed for other random graphs, of different sizes and choices of initial noise.

The second approach to ensure homegeneous intensities is by setting $P_m = P + 8n^m_{\rm NB}J^2/\gamma$ at each site. We highlight that such a nonuniform pump scheme is manifestly different from the ones considered in Refs. [29,30] as in our case the proper values of P_m are *a priori* known.

B. Ising graphs

Upon introducing a nonlinear loss on the "connecting" sites ($\Gamma'_{\rm NL} > 0$), a further symmetry breaking appears, that is the behavior illustrated in Fig. 3(b) emerges. The system still attains a stationary state, however, after approaching the intensity I_0 the "spin" sites coalesce their phases to one of two values, corresponding to $\mathbb{Z}_2$ freedom at each site. That is, the system develops into an effective Ising state. In Appendix A, we show how these Ising configurations remain fixed points of the nonlinear dynamics in presence of such ($\Gamma'_{\rm NL} > 0$).

III. OPTIMIZING SPIN MODELS

A. Extracting the spin-model energy

We have discussed how a random spin configuration of either an *XY*- or Ising-type Hamiltonian can form in the coupled cavity system. Considering the example of exciton polaritons, the states form on a timescale of picoseconds (or even shorter in some materials) and hence by using a pulsed-operation scheme, it is possible to sample a few trillion states in seconds in subsequent pulses $j = 1 \ldots N_{\rm pulses}$. However, so far the discussed scheme does not distinguish these many states.

Let us recap that for each pair of spins (n, m) connected in the original graphs, the corresponding "spin" sites ψ_n and ψ_m are coupled through a pair of "connecting" sites χ^S_{nm} and χ^A_{nm}. In the limit $\Gamma'_{\rm NL} = 0$, giving *XY* model states, the stationary intensities are

$$|\chi^{S,A}_{nm}|^2 = \frac{8J^2}{\gamma^2} I_0 \left(1 \pm \cos\left(\phi_n - \phi_m\right)\right), \tag{7}$$

where the $+$ sign applies to the χ^S_{nm} and $-$ to χ^A_{nm}. (The Ising case involves a simple rescaling, as shown in Appendix A.)

Defining $E_{\rm spin}$ by Eq. (1), we immediately see that

$$E_{\rm spin} \propto -\sum_{\langle nm\rangle} |\chi^X_{nm}|^2 + C, \tag{8}$$

where $X = S, A$ for ferromagnetic or antiferromagnetic coupling, respectively, and C is an irrelevant constant offset. The key feature is that the configuration that minimizes $E_{\rm spin}$ also maximizes $|\chi^X_{nm}|^2$, a quantity that can be easily accessed in experiment by summing emission intensity from specific "connecting" sites.

B. Reaching the ground state

Having completed the mapping, we now turn towards the protocol of finding the ground state, which has lowest $E_{\rm spin}$, or, equivalently, highest $\sum_{<nm>} |\chi^X_{nm}|^2$.

We will work in a pulsed setup, and thus define a periodic sequence of operations $j = 1 \ldots N_{\rm pulses}$. Each period j contains two stages, a "readout" stage and a "feedback" stage. We also define a real function $\mu(j)$, that increases linearly (or at least monotonically) with pulse number j.

1. Readout stage

During the first half of the period, the system evolves according to Eq. (3) with a fixed "spin" site gain $P = P_r$, during which a stationary state spin state is formed, such as the ones in Fig. 3. Then, also the "coupling" site intensities, Eq. (7), are extracted to obtain $\sum_{<nm>} |\chi^X_{nm}|^2$.

2. Feedback stage

During the second half of the period, one pumps the "spin" sites with a gain

$$P_f := \mu(j) \sum_{<nm>} |\chi^X_{nm}|^2, \tag{9}$$

everything else remaining the same. Unlike P_r in the readout state, P_f in the feedback stage is thus different for each pulse. Based on this value of P_f for the pulse, two situations can occur.

As long as P_f is sufficiently small, the condensate vanishes and the next pulse $j+1$ forms another one with different phases. This means that the system stochastically samples different spin states many times across the pulses j. By choosing $\mu(0)$ to be sufficiently low, we can always ensure that this situation occurs for the initial pulses.

Now, we have considered the parameter $\mu(j)$ to rise slowly with pulse count j. This will lead at some point for P_f to be sufficiently large for the second situation to occur. In this, the condensate is maintained at substantial intensity, large enough for the spin configuration to survive until the next pulse $j+1$.

If $\mu(j)$ is increased slowly enough, this is guaranteed to happen first when E_{spin} is minimal, as per the definition of Eq. (9). Furthermore, the fact that $\mu(j)$ is monotonically increasing, ensures that the survival of the spin configuration corresponding to this pulse continues throughout all subsequent pulses.

In Fig. 4, we show how this picture is confirmed numerically for both the *XY* and Ising models. The first three panels for each model show the effect of applying the procedure above to an individual spin graph, as simulated by Eq. (3). The effect of losing phase coherence below threshold is included by adding a small inhomogeneous random noise at the end of each feedback phase. As desired, after a certain number of pulses the system settles to an effective low-energy state due to the feedback scheme. This is only possible because of the correlation between the intensities of the S and A sets of "connecting" sites with the effective spin energy E_{spin}, which is shown in panels (b),(f). The obtained effective energy distributions are plotted in panels (c),(g) and compared to the distribution attained with a brute-force search. While the photonic simulator initially samples across the same distribution, a sharp peak emerges at the optimum (lowest) energy, which would grow in size if more pulses in the sequence were considered.

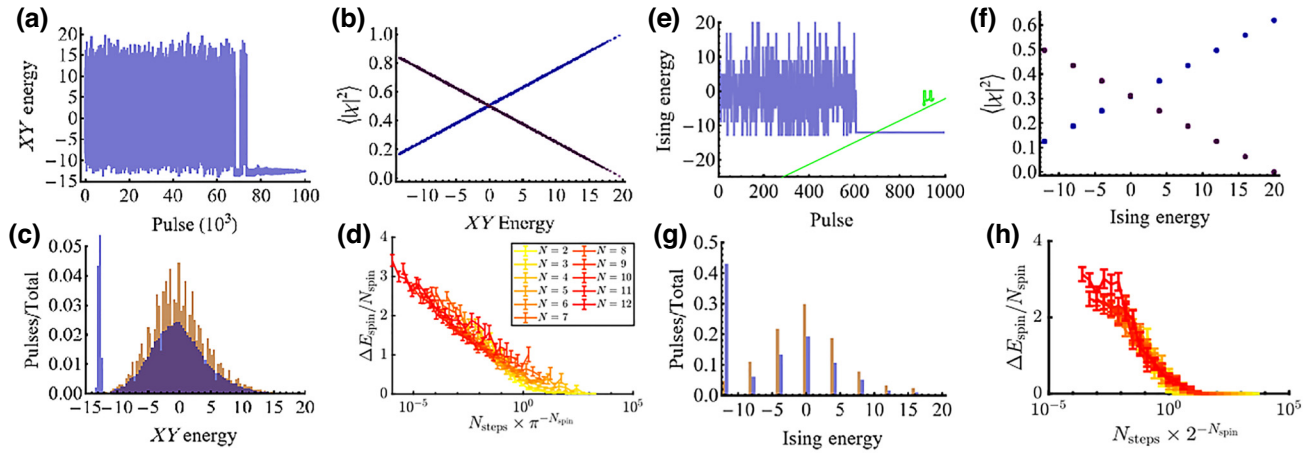

FIG. 4. Option 1 (all in one picture). Solving *XY* (a)–(d) and Ising (e)–(h) graphs. Panels (a)–(c)[(e)–(g)] depict the solution of the same random *XY* [Ising] graph and parameters (with P_r taking the value of P) of (3). (a)[(e)] The spin energy stabilizes when the feedback strength $P_f \propto \mu(j)$ becomes sufficiently strong. An example of a rising $\mu(j)$ is schematically added. (b)[(f)] as analytically predicted, E_{spin} is directly proportional to $\langle|\chi|^2\rangle$, where $\langle\cdot\rangle$ denotes the spatial average, selecting either χ^S or χ^A out of every coupling—allowing the scheme to work. (c)[(g)] Compares the distribution of *XY* [Ising] energies E_{spin} from the photonic simulator across pulses j (blue) with the raw density of states (as obtained from a brute-force search) (orange). These results show that the ground-state solution is exactly found, and as the simulator remains in this configuration, it forms a peak, which keeps on growing indefinitely. This behavior was verified for numerous individual graphs (d)[(e)] Statistics in the performance of different random graphs at multiple sizes, in finite time. Depicted is the excess energy above the true ground state ΔE_{spin} as a function of a rescaled number of pulses (yellow-red for different graph sizes $N_{\text{sites}} = 2-12$, each datapoint is the average over 30 graphs). Each curve shows that ΔE_{spin} and hence the distance from the true ground state becomes vanishingly small for sufficient pulses. The collapse for different sizes demonstrates the scaling behavior that allows one to extrapolate that the scheme would apply to graphs of arbitrary size. For these graphs, 50% all-to-all connectivity was chosen, which in turn has 50% ferromagnetic or antiferromagnetic coupling, reflecting realistic large graph problems. To compensate for external losses, in the *XY* case (d) extra dangling sites were used in combination with offset in P_r, P_f, while in the Ising case (h) only the offset was used without extra dangling sites. Results of the Ising case are less noisy since the spin states remain gapped (arbitrary perturbations would not lead to other configurations). All pulses used a total duration of $1000\Gamma_{\text{NL}}^{-1}$.

Now that we have illustrated the workings of the mechanism for an individual graph, we proceed to verify that it generalizes well to arbitrary graphs of different sizes [(d),(h)]. We tested graph sizes of $N = 2 - 12$ spins, with 30 random variations each. For the individual graph sizes, we see a steady decay of the excess energy above the true ground state to zero, meaning that all distance metrics to the true ground state must also decay, and highlighting that the ground state can be exactly obtained with a sufficient amount of pulses. While the number of pulses to achieve a certain accuracy increases exponentially with system size (as expected for an NP-hard problem) good collapse of the rescaled results emerges. This allows us to extrapolate the validity to the (thermodynamic) limit of arbitrarily large spin-glass graphs.

IV. CONCLUSIONS

Analog spin solvers hold great prospect as an emerging technology to solve complex computational problems efficiently. Despite a large amount of work in this area, there has been a major limitation of this principle, in that the optics-to-spin mapping becomes invalid due to heterogeneity of the optical amplitudes. Here, we have introduced an alternative scheme with coupled optical resonators (e.g. cavities with gain media or exciton polaritons). Depending on a parameter, this scheme is able to solve both *XY* or Ising spin problems. Of note, the scheme keeps the intensities completely homogeneous and is thus devoid of the aforementioned amplitude heterogeneity. This makes it possible for arbitrarily large spin-graph problems to be solved without bias.

ACKNOWLEDGMENTS

We gratefully acknowledge interesting discussions with N.G. Berloff, O. Kyriienko, M. Wouters and M. Weitz. W.V. and T.C.H.L. were supported by the Singaporean Ministry Education, via the Tier 2 Grant No. MOE-T2EP50121-0020 and Tier 3 Grant No. MOE2018-368-T3-1-002. M.M. and P.D. acknowledge support from Polish National Science Center Grant No. 2021/43/B/ST3/00752.

APPENDIX: ROLE OF Γ'_{nl} AND THE ISING CASE

To understand better how the choice of $\Gamma'_{\rm NL}$ determines *XY* or Ising-type behavior, let us again consider the plaquette of two "spin" cavities $\psi_{1,2}$ representing spins coupled in parallel by two "connecting" cavities $\chi^{S/A}$. We write $\psi_1 = \sqrt{n_1}e^{i\phi_1}$ and consider the evolution of the phase, yielding,

$$\frac{\partial\psi_1}{\partial t} + \frac{\partial\psi_1^*}{\partial t} = \frac{\cos\phi_1}{\sqrt{n_1}}\frac{\partial n_1}{\partial t} + 2\sqrt{n_1}\frac{\partial\cos\phi_1}{\partial t} \tag{A1}$$

The terms in Eq. (A1) can be evaluated as

$$\begin{aligned}\frac{\partial\psi_1}{\partial t} + \frac{\partial\psi_1^*}{\partial t} &= (P - \gamma - 2n_1\Gamma_{\rm NL})\sqrt{n_1}\cos\phi_1 \\ &\quad + iJ\left(\chi^S + \chi^A - \chi^{S*} - \chi_2^{A*}\right), \qquad \text{(A2)}\\ \frac{\partial n_1}{\partial t} &= (P - \gamma - 2n_1\Gamma_{\rm NL})\, n_1 \\ &\quad + iJ\left(\chi^S + \chi^A\right)\psi_1^* - iJ\left(\chi^{S*} + \chi^{A*}\right)\psi_1. \qquad \text{(A3)}\end{aligned}$$

Equation (A1) can then be written as

$$\begin{aligned}&iJ\left(\chi^S + \chi^A - \chi^{S*} - \chi^{A*}\right) - iJ\frac{\cos\phi_1}{\sqrt{n_1}}\left(\chi^S + \chi^A\right)\psi_1^* \\ &\quad + iJ\frac{\cos\phi_1}{\sqrt{n_1}}\left(\chi^{S*} + \chi^{A*}\right)\psi_1 = 2\sqrt{n_1}\frac{\partial\cos\phi_1}{\partial t}. \qquad \text{(A4)}\end{aligned}$$

Let us assume that $\chi^{S,A}$ follows its stationary value, which is given by a similar equation to Eq. (5), but here we allow for $\Gamma'_{\rm NL} \neq 0$:

$$\chi^{S,A} = \frac{2iJ\left(\psi_1 \pm \psi_2\right)}{\gamma + 2\Gamma'_{\rm NL}|\chi_{S,A}|^2}. \tag{A5}$$

Equation (A4) becomes

$$\begin{aligned}&-2J^2\frac{\psi_1 + \psi_2}{\gamma + 2\Gamma'_{\rm NL}|\chi^S|^2} - 2J^2\frac{\psi_1 - \psi_2}{\gamma + 2\Gamma'_{\rm NL}|\chi_A|^2} \\ &-2J^2\frac{\psi_1^* + \psi_2^*}{\gamma + 2\Gamma'_{\rm NL}|\chi^S|^2} - 2J^2\frac{\psi_1^* - \psi_2^*}{\gamma + 2\Gamma'_{\rm NL}|\chi^A|^2} \\ &+\frac{2J^2\cos\phi_1}{\sqrt{n_1}}\left(\frac{\psi_1 + \psi_2}{\gamma + 2\Gamma'_{\rm NL}|\chi^S|^2} + \frac{\psi_1 - \psi_2}{\gamma + 2\Gamma'_{\rm NL}|\chi^A|^2}\right)\psi_1^* \\ &+\frac{2J^2\cos\phi_1}{\sqrt{n_1}}\left(\frac{\psi_1^* + \psi_2^*}{\gamma + 2\Gamma'_{\rm NL}|\chi^S|^2} + \frac{\psi_1^* - \psi_2^*}{\gamma + 2\Gamma'_{\rm NL}|\chi^A|^2}\right)\psi_1 \\ &= 2\sqrt{n_1}\frac{\partial\cos\phi_1}{\partial t}. \qquad \text{(A6)}\end{aligned}$$

In the case of $\Gamma'_{\rm NL} = 0$ all the denominators are equal, the ψ_2 terms cancel, and the left-hand side of the equation is zero. In this case, the phase ϕ_1 becomes constant and a stationary state is allowed without needing a specific value of ϕ_1. Similar arguments hold for ϕ_2, which can take any phase independent of ϕ_1, giving *XY*-type behavior.

In the case of $\Gamma'_{\rm NL} \neq 0$ the denominators in Eq. (A6) are not generally equal and we have a finite value of $\partial\cos\phi_1/\partial t$, implying that the phase continues evolving. However, in the special cases $\psi_1 = \pm\psi_2$, it is readily seen that the terms on the left-hand side of Eq. (A6) again vanish. Consequently, we find that the system can only reach a stable stationary state when $\psi_1 = \pm\psi_2$. Thus, we obtain an Ising-type behavior. We note that this solution implies that

one of the $\chi^{S,A}$ of each pair reaches a finite intensity $|\chi^X|^2$ with a phase difference $\pi/2$ while the other is empty. As in the *XY* case, this solution prevents any polariton current from ψ_1 to ψ_2, allowing to keep the amplitude homogeneous again. By inserting Eq. (A5) in the Gross-Pitaevskii Eq. (3), we obtain the algebraic equation

$$\Gamma'_{\mathrm{NL}}|\chi^X|^3 + \frac{\gamma}{2}|\chi^X| - 2J\sqrt{\frac{P-\gamma}{2\Gamma_{\mathrm{NL}}}} = 0. \tag{A7}$$

Solving for $|\chi^X|$, we can correct I_0 once more, in the case of n_{nb} neighbors this becomes

$$I_{0,\mathrm{mod}} := |\psi_n|^2 = \frac{P-\gamma}{2\Gamma_{\mathrm{NL}}} - \frac{4n_{\mathrm{nb}}J^2}{(\gamma + 2|\chi^X|^2\Gamma'_{\mathrm{NL}})\Gamma_{\mathrm{NL}}}. \tag{A8}$$

One way to ensure that this quantity remains homogeneous is by adapting the incoherent pump P to

$$P \to P_n = P + 8n_{\mathrm{nb}}J^2/\left(\gamma + 2|\chi^X|^2\Gamma'_{\mathrm{NL}}\right). \tag{A9}$$

Note that we have some additional numerical evidence (not presented) that a similar scheme also applies with a coherent nonlinearity in the "connecting" sites instead of the nonlinear losses ($\Gamma'_{\mathrm{NL}} \to i\alpha'$).

[1] Dagmar Bruß and Gerd Leuchs, *Lectures on Quantum Information* (Wiley-VCH, Weinheim, 2018).

[2] Raul Rojas, *Neural Networks: A Systematic Introduction* (Springer, Berlin, 1996).

[3] Ehud Altman *et al.*, Quantum simulators: Architectures and opportunities, PRX Quantum **2**, 017003 (2021).

[4] Giorgio Parisi, Nobel lecture: Multiple equilibria, Rev. Mod. Phys. **95**, 030501 (2023).

[5] Bei Zeng, *Quantum Information Meets Quantum Matter: From Quantum Entanglement to Topological Phases of Many-Body Systems* (Springer, New York, 2019).

[6] Daniel L. Stein and Charles M. Newman, *Spin Glasses and Complexity* (Princeton University Press, Princeton, 2013).

[7] D. Aharonov, W. van Dam, J. Kempe, Z. Landau, S. Lloyd, and O. Regev, in *45th Annual IEEE Symposium on Foundations of Computer Science* (IEEE, Rome, 2004), p. 42.

[8] Naeimeh Mohseni, Peter L. McMahon, and Tim Byrnes, Ising machines as hardware solvers of combinatorial optimization problems, Nat. Rev. Phys. **4**, 363 (2022).

[9] Alexey Kavokin, Timothy C. H. Liew, Christian Schneider, Pavlos G. Lagoudakis, Sebastian Klembt, and Sven Hoefling, Polariton condensates for classical and quantum computing, Nat. Rev. Phys. **4**, 435 (2022).

[10] Nikita Stroev and Natalia G. Berloff, Analog photonics computing for information processing, inference, and optimization, Adv. Quantum Technol. **n/a**, 2300055 (2023).

[11] Andrzej Opala and Michał Matuszewski, Harnessing exciton-polaritons for digital computing, neuromorphic computing, and optimization, Opt. Mater. Express **13**, 2674 (2023).

[12] O. Kyriienko, H. Sigurdsson, and T. C. H. Liew, Probabilistic solving of *np*-hard problems with bistable nonlinear optical networks, Phys. Rev. B **99**, 195301 (2019).

[13] Helgi Sigurdsson, Oleksandr Kyriienko, Kevin Dini, and Timothy C. H. Liew, All-to-all intramodal condensate coupling by multifrequency excitation of polaritons, ACS Photonics **6**, 123 (2019).

[14] M. Leonetti, E. Hrmannrmann, L. Leuzzi, G. Parisi, and G. Ruocco, Optical computation of a spin glass dynamics with tunable complexity, Proc. Natl. Acad. Sci. **118**, e2015207118 (2021).

[15] H. Ohadi, A. J. Ramsay, H. Sigurdsson, Y. del Valle-Inclan Redondo, S. I. Tsintzos, Z. Hatzopoulos, T. C. H. Liew, I. A. Shelykh, Y. G. Rubo, P. G. Savvidis, and J. J. Baumberg, Spin order and phase transitions in chains of polariton condensates, Phys. Rev. Lett. **119**, 067401 (2017).

[16] Natalia G. Berloff, Matteo Silva, Kirill Kalinin, Alexis Askitopoulos, Julian D. Töpfer, Pasquale Cilibrizzi, Wolfgang Langbein, and Pavlos G. Lagoudakis, Realizing the classical XY Hamiltonian in polariton simulators, Nat Mater. **16**, 1120 (2017).

[17] J. Struck, C. Ölschläger, R. Le Targat, P. Soltan-Panahi, A. Eckardt, M. Lewenstein, P. Windpassinger, and K. Sengstock, Quantum simulation of frustrated classical magnetism in triangular optical lattices, Science **333**, 996 (2011).

[18] Micha Nixon, Eitan Ronen, Asher A. Friesem, and Nir Davidson, Observing geometric frustration with thousands of coupled lasers, Phys. Rev. Lett. **110**, 184102 (2013).

[19] Chris Toebes, Mario Vretenar, and Jan Klaers, Dispersive and dissipative coupling of photon Bose-Einstein condensates, Commun. Phys. **5**, 59 (2022).

[20] Alireza Marandi, Zhe Wang, Kenta Takata, Robert L. Byer, and Yoshihisa Yamamoto, Network of time-multiplexed optical parametric oscillators as a coherent Ising machine, Nat. Photonics **8**, 937 (2014).

[21] Marcello Calvanese Strinati, Davide Pierangeli, and Claudio Conti, All-optical scalable spatial coherent Ising machine, Phys. Rev. Appl. **16**, 054022 (2021).

[22] Hayato Goto, Bifurcation-based adiabatic quantum computation with a nonlinear oscillator network, Sci. Rep. **6**, 21686 (2016).

[23] Wouter Verstraelen and Michiel Wouters, Classical critical dynamics in quadratically driven Kerr resonators, Phys. Rev. A **101**, 043826 (2020).

[24] D. Pierangeli, G. Marcucci, and C. Conti, Large-scale photonic Ising machine by spatial light modulation, Phys. Rev. Lett. **122**, 213902 (2019).

[25] Kirill P. Kalinin and Natalia G. Berloff, Simulating Ising and *n*-state planar Potts models and external fields with nonequilibrium condensates, Phys. Rev. Lett. **121**, 235302 (2018).

[26] Toshimori Honjo, Tomohiro Sonobe, Kensuke Inaba, Takahiro Inagaki, Takuya Ikuta, Yasuhiro Yamada, Takushi Kazama, Koji Enbutsu, Takeshi Umeki, and Ryoichi Kasahara *et al.*, 100 000-spin coherent Ising machine, Sci. Adv. **7**, eabh0952 (2021).

[27] Marcello Calvanese Strinati, Leon Bello, Emanuele G. Dalla Torre, and Avi Pe'er, Can nonlinear parametric

oscillators solve random Ising models?, Phys. Rev. Lett. **126**, 143901 (2021).

[28] Fabian Böhm, Thomas Van Vaerenbergh, Guy Verschaffelt, and Guy Van der Sande, Order-of-magnitude differences in computational performance of analog Ising machines induced by the choice of nonlinearity, Commun. Phys. **4**, 149 (2021).

[29] Kirill P. Kalinin and Natalia G. Berloff, Global optimization of spin Hamiltonians with gain-dissipative systems, Sci. Rep. **8**, 17791 (2018).

[30] Timothée Leleu, Yoshihisa Yamamoto, Peter L. McMahon, and Kazuyuki Aihara, Destabilization of local minima in analog spin systems by correction of amplitude heterogeneity, Phys. Rev. Lett. **122**, 040607 (2019).

[31] James S. Cummins, Hayder Salman, and Natalia G. Berloff, Classical vs quantum annealing and manifold reduction in soft-spin minimizers of Ising Hamiltonians, arXiv:2311.17359 (2023).

[32] Na Young Kim, Kenichiro Kusudo, Congjun Wu, Naoyuki Masumoto, Andreas Löffler, Sven Höfling, Norio Kumada, Lukas Worschech, Alfred Forchel, and Yoshihisa Yamamoto, Dynamical d-wave condensation of exciton–polaritons in a two-dimensional square-lattice potential, Nat. Phys. **7**, 681 (2011).

[33] T. Jacqmin, I. Carusotto, I. Sagnes, M. Abbarchi, D. D. Solnyshkov, G. Malpuech, E. Galopin, A. Lemaître, J. Bloch, and A. Amo, Direct observation of Dirac cones and a flatband in a honeycomb lattice for polaritons, Phys. Rev. Lett. **112**, 116402 (2014).

[34] K. Winkler, O. A. Egorov, I. G. Savenko, X. Ma, E. Estrecho, T. Gao, S. Müller, M. Kamp, T. C. H. Liew, E. A. Ostrovskaya, S. Höfling, and C. Schneider, Collective state transitions of exciton-polaritons loaded into a periodic potential, Phys. Rev. B **93**, 121303 (2016).

[35] Alberto Amo and Jacqueline Bloch, Exciton-polaritons in lattices: A non-linear photonic simulator, C. R. Phys. **17**, 934 (2016), polariton physics / Physique des polaritons.

[36] Na Young Kim and Yoshihisa Yamamoto, in *Quantum Simulations with Photons and Polaritons: Merging Quantum Optics with Condensed Matter Physics*, edited by Dimitris G. Angelakis (Springer International Publishing, Cham, 2017), p. 91.

[37] Kirill P. Kalinin and Natalia G. Berloff, Polaritonic network as a paradigm for dynamics of coupled oscillators, Phys. Rev. B **100**, 245306 (2019).

[38] Kirill P. Kalinin, Alberto Amo, Jacqueline Bloch, and Natalia G. Berloff, Polaritonic XY-Ising machine, Nanophotonics **9**, 4127 (2020).

[39] Kirill P. Kalinin and Natalia G. Berloff, Networks of non-equilibrium condensates for global optimization, New J. Phys. **20**, 113023 (2018).

[40] Jiangang Feng, Jun Wang, Antonio Fieramosca, Ruiqi Bao, Jiaxin Zhao, Rui Su, Yutian Peng, Timothy C. H. Liew, Daniele Sanvitto, and Qihua Xiong, All-optical switching based on interacting exciton polaritons in self-assembled perovskite microwires, Sci. Adv. **7**, eabj6627 (2021).

[41] Fei Chen, Hang Zhou, Hui Li, Junhui Cao, Song Luo, Zheng Sun, Zhe Zhang, Ziqiu Shao, Fenghao Sun, Beier Zhou, Hongxing Dong, Huailiang Xu, Hongxing Xu, Alexey Kavokin, Zhanghai Chen, and Jian Wu, Femtosecond dynamics of a polariton bosonic cascade at room temperature, Nano Lett. **22**, 2023 (2022).

[42] Michiel Wouters, Synchronized and desynchronized phases of coupled nonequilibrium exciton-polariton condensates, Phys. Rev. B **77**, 121302 (2008).

[43] John P. Moroney and Paul R. Eastham, Synchronization in disordered oscillator lattices: Nonequilibrium phase transition for driven-dissipative bosons, Phys. Rev. Res. **3**, 043092 (2021).

[44] H. Ohadi, R. L. Gregory, T. Freegarde, Y. G. Rubo, A. V. Kavokin, N. G. Berloff, and P. G. Lagoudakis, Nontrivial phase coupling in polariton multiplets, Phys. Rev. X **6**, 031032 (2016).

[45] Piotr Stępnicki and Michał Matuszewski, Tight-binding model for exciton-polariton condensates in external potentials, Phys. Rev. A **88**, 033626 (2013).

[46] Iacopo Carusotto and Cristiano Ciuti, Quantum fluids of light, Rev. Mod. Phys. **85**, 299 (2013).

[47] Jonathan Keeling and Natalia G. Berloff, Spontaneous rotating vortex lattices in a pumped decaying condensate, Phys. Rev. Lett. **100**, 250401 (2008).

[48] Philippe Grelu and Nail Akhmediev, Dissipative solitons for mode-locked lasers, Nat. Photonics **6**, 84 (2012).

[49] M. R. Garey, D. S. Johnson, and L. Stockmeyer, Some simplified np-complete graph problems, Theor. Comput. Sci. **1**, 237 (1976).

[50] Gemma De las Cuevas and Toby S. Cubitt, Simple universal models capture all classical spin physics, Science **351**, 1180 (2016).